Scaling of strength and ductility in bioinspired brick and mortar composites

David V. Wilbrink,[1] Marcel Utz,[2] Robert O. Ritchie,[3] and Matthew R. Begley[4,a]
[1]*Mechanical Engineering, Eindhoven University of Technology, Eindhoven, The Netherlands*
[2]*Mechanical and Aerospace Engineering, University of Virginia, Charlottesville, Virginia 22904, USA*
[3]*Materials Science and Engineering, University of California, Berkeley, California 94720, USA*
[4]*Mechanical Engineering, University of California, Santa Barbara, California 93104, USA*

This paper provides scaling relationships between constituent properties and the uniaxial tensile response of synthetic "brick and mortar" composite materials inspired by nacre. The macroscopic strength and ductility (work of fracture) are predicted in terms of the brick properties (size, strength, and layout) and interface cohesive properties (e.g., maximum shear and normal stresses and separations). The results illustrate the trade-off between increasing strength and decreasing ductility with the increasing aspect ratio of the bricks. The models can be used to identify optimum mortar properties that maximize toughness for a given brick strength. © *2010 American Institute of Physics*. [doi:10.1063/1.3499294]

The development of freeze-casting techniques to synthesize bioinspired composites of ceramic "bricks" and polymeric "mortar" creates significant opportunities to create strong, lightweight and tough materials.[1] Like nacre (abalone shell), the high strength of these composites is almost entirely due to the ceramic (mineral) phase; however, they additionally display remarkable toughness because limited sliding between the bricks acts to dissipate local stress concentrations, much like dislocation motion in metals or microcracking in bone. For synthetic materials, critical questions arise regarding how the constituents should be tailored to promote toughness while not undermining strength.

Here, we present a simple uniaxial model to identify the scaling relationships between constituent properties and the macroscopic composite strength and work to failure. Rather than predicting the complex behavior in biological materials,[2–5] the motivation for the present model is the need to identify combinations of mortar and brick properties that optimize the macroscopic response of synthetic materials. Currently, synthetic materials involve much higher volume fractions of the polymeric phase (e.g., 10%), and blocks with smaller aspect ratios than most biological systems. Hence, we adopt an idealized model that neglects details more relevant in biomineralized natural materials (such as molecular stretching, stiff bridging ligaments, or rough interfaces). In spirit, the approach is similar to composite modeling that utilizes atomistic-based cohesive laws describing the interaction between polymers and rigid particles.[6,7] However, since the interplay between interface bonding and inelastic polymer deformation has yet to be quantified for the present materials, we adopt a phenomenological cohesive law.[8] The law is quantitatively similar to van der Waals bonding when the peak stress and critical separation of the cohesive law are matched: the focus here is on the relationship between these parameters, brick geometry, and macroscopic response.

A schematic of the brick and mortar idealization used for the present model and the corresponding unit cell is shown in Fig. 1. All bricks are defined to have width w, height h, and rows of bricks overlap by s. It is assumed that the elastic stretching of the bricks is negligible compared to the displacements of the bricks relative to one another; hence, the bricks are treated as rigid. However, one can compute the maximum stress in a brick, which occurs just below each vertical mortar layer, at $x=0$ in Fig. 1(b). The mortar is represented using cohesive laws acting between adjacent brick interface: for simplicity, we assume the mortar thickness is much smaller than the brick dimensions. [Finite mortar layer thicknesses are shown in Fig. 1(b) for clarity.]

In the kinematics of the unit cell deformation [Fig. 1(b)], the bottom (reference) brick is considered fixed. The adjacent (cohesive) mortar layers experience purely horizontal displacements, such that the cohesive layers connecting adjacent rows are sheared, while the layers across vertical interfaces experience tension. While the total vertical gap that opens up between any two bricks is spatially uniform throughout the composite, the displacements of the two
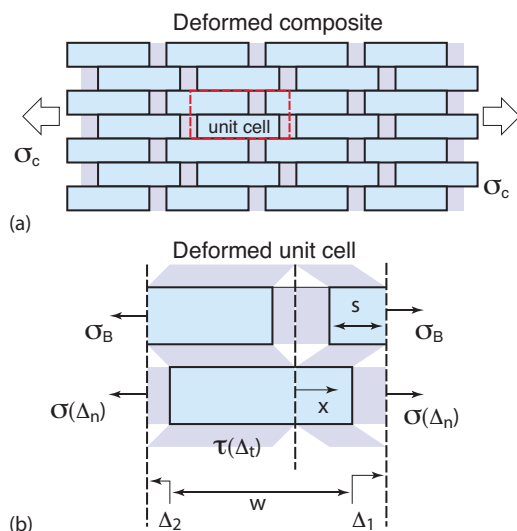

FIG. 1. (Color online) Schematic illustration of (a) the composite and (b) the unit cell used in the analysis.

---

[a]Author to whom correspondence should be addressed. Electronic mail: begley@engr.ucsb.edu.
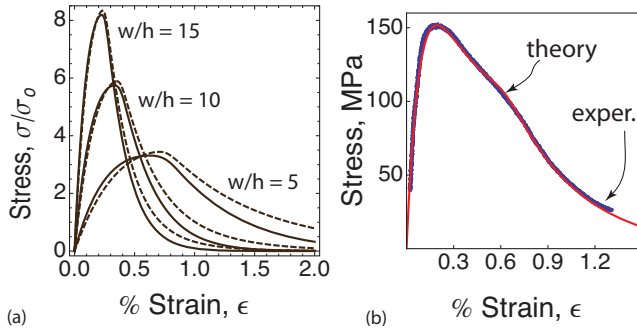
FIG. 2. (Color online) (a) Composite stress-strain relationships: illustrating the effect of brick aspect ratio w/h, for $s/w=0.49$ and $\tau_o=\sigma_o$: solid lines are for $\delta_{1c}=\delta_{2c}=0.02h$, dashed lines are for $\delta_{1c}=0.04h$, $\delta_{2c}=0.02h$. (b) Comparison of theory with previously published experiments (Ref. 1): $w=20\ \mu m$, $h=3\ \mu m$, $s/w=0.5$, $\sigma_o=102$ MPa, $\tau_o=28$ MPa, $\delta_{1c}=30$ nm, and $\delta_{2c}=75$ nm.

bricks within the unit cell are asymmetric. The top left brick in the unit cell is displaced by Δ_1 (i.e., for $x>0$), while the right is displaced by Δ_2 (i.e., for $x<0$). The composite macroscopic strain is defined by $\varepsilon=(\Delta_1+\Delta_2)/w$. Since the bottom brick is rigid and fixed, the displacements Δ_1 and Δ_2 reflect the *relative* displacements that are fed into the traction-displacement relation defining the cohesive interfaces.

To capture the phenomenon of cohesive layer rupture, the cohesive law is described as a nonmonotonic function of relative displacements, similar the stress-strain relationships illustrated in Fig. 2. The cohesive tractions along the vertical layers, $\sigma(\Delta_n)$, and along the horizontal layers, $\tau(\Delta_t)$, are prescribed as follows:[8]

$$\sigma = e\sigma_o\frac{\Delta_n}{\delta_{1c}}e^{-\Delta_n/\delta_{1c}}, \quad \tau = e\tau_o\frac{\Delta_t}{\delta_{2c}}e^{-\Delta_t/\delta_{2c}}, \tag{1}$$

where Δ_n is the relative normal displacement of the vertical interfaces, while Δ_t is the relative tangential (sliding) displacement of the horizontal interfaces. The peak cohesive stresses are given by σ_o and τ_o. The critical displacements required to reach the peak stresses are δ_{1c} and δ_{2c}. The corresponding work of separation of the cohesive layers is $W_i=e\sigma_o\delta_{1c}$ (vertical) and $W_i=e\tau_o\delta_{2c}$ (horizontal).

Using the kinematics described above and referring to the unit cell, the horizontal cohesive layers experience the shear displacements $\Delta_t=\Delta_1$ for $x>0$ and $\Delta_t=\Delta_2$ for $x<0$. For all vertical layers, the normal separation is given by $\Delta_n=\Delta_1+\Delta_2$. In the general case (i.e., $s\neq w/2$ and different critical displacements for shear and normal stresses), the shear and normal stresses reach a maximum at different stages of deformation. Force balance at each brick's origin implies that $\bar{s}\tau(\Delta_1)=(1-\bar{s})\tau(w\varepsilon-\Delta_1)$, where $\bar{s}=s/w$ and σ_B defines the maximum stress in the brick. This equation is used to determine Δ_1 at a prescribed level of macroscopic strain; Δ_2 is eliminated as a variable using the definition of the macroscopic strain. The brick stress is then computed as $\sigma_B=[2\bar{s}\tau(\Delta_1)+\sigma_n(w\varepsilon)]/2$. The average macroscopic composite stress, computed at a given vertical plane (e.g., $x=0$), is then $\sigma_c=(1/2)(\sigma_B+\sigma_o)$.

For the special case when $\bar{s}=0.5$, symmetry dictates that relative motions are described by the displacements $\Delta_1=\Delta_2=w\varepsilon/2$. If $\delta_{1c}=2\delta_{2c}$, the vertical and horizontal mortar layers will experience identical separations *relative to their control-*

ling length scale; i.e., $\Delta_n/\delta_{1c}=\Delta_t/\delta_{2c}$. In this case, the strength of the composite is dictated only by the maximum stresses of cohesive laws, σ_o and τ_o. For systems with strong bricks (as presumably the case with ceramic phase with small volumes), the optimum performance is obtained by tuning τ_o such that the peak stress in the bricks is just below their strength σ_B^f. In this case, the maximum work of fracture of the composite is obtained because full sliding "pull-out" of ceramic bricks will occur before brick failure. This optimum, with the observed failure strength of the composite $\sigma_c^f=1/2(\sigma_o+\sigma_B^f)$, is described by the following:

$$\tau_o^{\text{opt}} = \frac{h}{w}(\sigma_B^f-\sigma_o), \quad W_f = c\delta_{1c}\sigma_o\left[1+\frac{h}{w}\left(\frac{\sigma_B^f}{\sigma_o}-1\right)\right], \tag{2}$$

where σ_B^f is the failure stress of the ceramic bricks and W_f is the failure work per unit cross-sectional area. It should be emphasized that these results are valid regardless of the shape of the cohesive law; only the dimensionless constant c depends on the form of the cohesive law (here, $c\sim1.36$). This optimum illustrates that if the mortar is tailored to maximize strength, the toughness will decrease with brick aspect ratio $\bar{w}=w/h$. Note that the optimum composite failure stress scales as one-half the brick strength (presuming the mortar phase has limited strength), since at a given plane, loads are focused from the vertical gaps onto the adjacent bricks.

Regardless of whether or not the shear behavior of the mortar is tuned to the optimum outlined above, there is a fundamental trade-off between composite strength and ductility with increasing aspect ratio $\bar{w}$, as shown in Fig. 2(a) (for the case $\tau_o=\sigma_o$). As $\bar{w}$ increases, the maximum stress increases and the failure work (area under the curves, a measure for ductility) decreases. For large aspect ratios $\bar{w}$, this is true even when the mortar does not deform proportionally on the vertical and horizontal layers (i.e., when $2\delta_{1c}\neq\delta_{2c}$), since shear stresses dominate the composite response. This is illustrated in Fig. 2(a); only small changes in the composite response result from changing the critical normal displacement (δ_{1c}) by a factor 2.

In Fig. 2(b), the above the theory with $\bar{s}=0.5$ is compared with results from previously published experiments for a "brick and mortar composite" comprised of 85 wt % alumina and 15 wt % poly(methylmethacrylate).[1] Since the theory neglects elastic deformation of the bricks, the measured strains are adjusted by subtracting an estimate for the composite's elastic deformation. Figure 2(b) plots $\varepsilon=\varepsilon_{\text{exp}}-\sigma_{\text{exp}}/E_{\text{exp}}$, where ε_{exp} is the total experimental strain, and the experimental elastic modulus (at smalls strains) is $E_{\text{exp}}\approx50$ GPa. For the theory, the critical stresses and separations were used as fitting parameters (values listed in the caption). Good agreement is not surprising with four fitting parameters. However, there is a relatively narrow range of parameters that capture the data even crudely. It is worth noting scanning electron microscopy observations show damage localization,[1] i.e., brick failure and regions where local sliding is larger than the surrounding bricks. However, such observations are by their very nature local and it is difficult to detect more defuse submicron deformation; moreover, one anticipates abrupt drops in stress associated with the spread of a dominant defect. Using reasonable cohesive parameters, the present homogeneous deformation model is
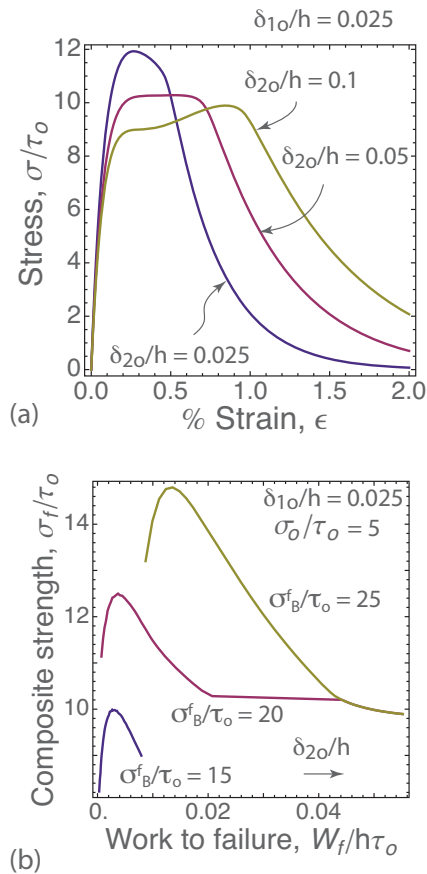
FIG. 3. (Color online) Results for $w/h=20$, $s/w=0.49$, $\sigma_o=5\tau_o$, and various combinations of critical displacements, and brick strength. (a) Composite strength is at a maximum when the shear and normal critical displacements are the same, implying an additive effect of shear and normal stresses: it then decreases as δ_{2c} increases, due to different strain levels associated with peak stress. (b) Plot of the composite strength vs failure work, illustrating the general trade-off between strength and ductility; along each curve from left to right, δ_{2o} increases.

in clear agreement with the gradual loss of load-carrying capacity seen in Fig. 2(b).

In fitting the model to the experiment, it is critical to use different values for normal and shear contributions. The model implies (for the experimental composite) that the normal stress (in the vertical cohesive layers) dominates the composite peak stress; the shear stress (in the horizontal layers) controls the softening behavior. Roughly, ±20% variations in σ_o and δ_{1c} lead to changes in similar proportion in the predictions near the first peak, and ±20% variations in τ_o and δ_{2c} lead to changes in similar proportion in the predictions in the softening portion of the response. The model suggests that the slight bump present at $\varepsilon \approx 0.7\%$ correlates with a peak in shear stress.

The model further implies that the slight "bump" seen in Fig. 2(b) at $\varepsilon \approx 0.7\%$ can be exaggerated to significantly increase the composite work to fracture, provided the critical shear sliding distance can be increased relative to that controlling normal separation. This is illustrated in Fig. 3(a) as follows: larger critical shear sliding distances lead to peak shear stresses at larger strains. Reasonably elevated composite strength is maintained over a large range of strains by creating a transition between small strain behavior dominated by normal stresses and large strain behavior dominated by shear stresses. The fundamental trade-off between

strength and failure work is unavoidable, however; Fig. 3(b) plots the correlation of composite strength and failure work, with the critical shear sliding distance as an implicit parameter that increases from left to right.

The highest strength is achieved when the critical sliding distances are nearly equal, as both cohesive layers contribute to load carrying capacity at the same level of macroscopic strain. This additive effect is lost when the critical shear sliding distance increases, though this increases the failure work. The results in Fig. 3(b) also illustrate the general implications of the model for scenarios involving brick failure. (In these cases, the composite strength is taken as the maximum reached such that the brick stress is below its strength. The composite failure work is computed up until the point of brick failure.) In Fig. 3, low brick strength implies that the composite fails before exhibiting pull-out, limiting both strength and failure work. The results in Fig. 3 for $\sigma_B^f=20\tau_o$ illustrate a sharp increase in failure work for conditions that narrowly avoid brick failure (as described earlier); when the critical shear sliding distance reaches a critical value of $\delta_{2c}/h \sim 0.02$, the failure work jumps because brick failure is just avoided, while the composite strength is relatively constant. However, even if brick failure is avoided [e.g., $\sigma_B^f=25\tau_o$ in Fig. 3(b)], increasing the failure work to significant levels leads to a concomitant decrease in composite strength.

The present results, combined with the assumption that the critical distances δ_{1c} and δ_{2c} will scale with the mortar thickness, suggest that there is an optimal mortar thickness; it must be small enough to avoid brick failure driven by the additive effect of shear and normal stresses, but large enough to ensure effective load transfer. Although the present model is clearly able to predict mechanical behavior consistent with experiments, future modeling is needed to rigorously connect critical cohesive properties to microscale and nanoscale properties, such as bond strength and polymer yield strength. The present results are informative, however; if the peak composite stress is governed by mortar yield strength, say ~ 50 MPa, and the brick strength is ~ 1 GPa, the optimal value of critical sliding displacement is ~ 75 nm (similar to that inferred from the above matching with experiments) for bricks measuring 20 by 1 μm. These properties would lead to composite strengths of ~ 500 MPa, with failure work on the order of 40 kJ/m^2. Relative to the existing materials shown in Fig. 2(b), this would represent a factor of 3 improvement in strength, and a factor of 3 improvement in toughness.

[1]E. Munch, M. E. Launey, D. H. Alsem, E. Saiz, A. P. Tomsia, and R. O. Ritchie, Science **322**, 1516 (2008).
[2]J. D. Currey, Proc. R. Soc., London, Ser. B **196**, 443 (1977).
[3]A. P. Jackson, J. F. V. Vincent, and R. M. Turner, Proc. R. Soc., London, Ser. B **234**, 415 (1988).
[4]B. L. Smith, T. E. Schäffer, M. Viani, J. B. Thompson, N. A. Frederick, J. Kindt, A. Belcher, G. D. Stucky, D. E. Morse, and P. K. Hansma, Nature (London) **399**, 761 (1999).
[5]S. Weiner and H. Lowenstam, Crit. Rev. Biochem. Mol. Biol. **20**, 365 (1986).
[6]H. Tan, L. Y. Jiang, Y. Huang, B. Liu, and K. C. Hwang, Compos. Sci. Technol. **67**, 2941 (2007).
[7]L. Y. Jiang, Y. Huang, H. Jiang, G. Ravichandran, H. Gao, K. C. Hwang, and B. Liu, J. Mech. Phys. Solids **54**, 2436 (2006).
[8]X.-P. Xu and A. Needleman, J. Mech. Phys. Solids **42**, 1397 (1994).